

Article

Cu/CuO-Decorated Peanut-Shell-Derived Biochar for the Efficient Degradation of Tetracycline via Peroxymonosulfate Activation

Jianhui Zhao ¹, Huan Li ¹, Yuanzhou Wang ¹, Jingjie Yu ¹, Ning Li ^{2,*} and Shaopo Wang ^{1,*}¹ School of Environmental and Municipal Engineering, Tianjin Chengjian University, Tianjin 300384, China² School of Environmental Science and Engineering, Tianjin University, Tianjin 300072, China

* Correspondence: liningec@tju.edu.cn (N.L.); wsp@tcu.edu.cn (S.W.); Tel.: +86-(022)87402072 (N.L.); +86-(022)23085117 (S.W.)

Abstract: Biochar (BC) usually has abundant surface functional groups, well-developed pore structures and high specific surface areas, which can combine with transition metals for peroxymonosulfate (PMS) activation to degrade organics. In this paper, BC modified with Cu/CuO was prepared by a modified impregnation pyrolysis method using peanut shells as raw materials. The morphology, structure and physicochemical properties were analyzed. Results showed that the originally smooth BC surface was modified into a rough structure with distributed metal particles, and the specific surface area of the modified Cu/CuO-BC700 (i.e., Cu/CuO-BC) increased from the initial 22.57 to 192.64 m²/g. The Cu/CuO-BC was employed for PMS activation and tetracycline (TC) degradation, achieving a removal efficiency of 93.2% at TC initial concentration 20 mg/L, PMS concentration 0.5 mM and catalyst dosage 0.1 g/L after 30 min. The influence of co-existing anions in the actual water on TC degradation followed the order of HCO₃⁻ > H₂PO₄⁻ > Cl⁻, and HA had an inhibitory effect on TC degradation. A variety of active species participated in TC degradation, and the free radical pathway played a dominant role. Furthermore, the Cu/CuO-BC could maintain the degradation efficiency of TC up to 80% even after five consecutive cycles. The Cu/CuO-BC maintained high activity through redox reactions between catalytically generated active species and the cycling of metal ions (Cu⁺/Cu²⁺).

Keywords: Cu/CuO; modified biochar; peroxymonosulfate; active species; tetracycline

Citation: Zhao, J.; Li, H.; Wang, Y.; Yu, J.; Li, N.; Wang, S. Cu/CuO-Decorated

Peanut-Shell-Derived Biochar for the Efficient Degradation of Tetracycline via Peroxymonosulfate Activation.

Catalysts **2023**, *13*, 1246. <https://doi.org/10.3390/catal13091246>

Academic Editors: Oh Wen Da, Yueping Bao and Chong Wang

Received: 23 July 2023

Revised: 22 August 2023

Accepted: 25 August 2023

Published: 28 August 2023



Copyright: © 2023 by the authors. Licensee MDPI, Basel, Switzerland. This article is an open access article distributed under the terms and conditions of the Creative Commons Attribution (CC BY) license (<https://creativecommons.org/licenses/by/4.0/>).

1. Introduction

Tetracyclines (TCs) with strong bacterial inhibitory action are widely used for the prevention and treatment of human and animal diseases [1]. TCs, which are detected in surface water, groundwater and soil as an emerging contaminant through multiple migration pathways, cannot be fully metabolized in animals [2,3]. The relevant risk assessment shows that human daily intake of antibiotics (containing TCs) through drinking water is 1 µg/kg [4]. Even if the concentration of ng/L–µg/L of TCs exists in water for a long time, it still poses a great danger to human health and environmental security [5]. Therefore, the safe and highly effective removal of TCs is urgent.

Various methods, including biological treatment, adsorption, membrane filtration and advanced oxidation, are applied to remove TCs from water [6–9]. Biological methods have high treatment capacity and mild reaction conditions. Nevertheless, microorganisms in water are subject to massive death when treating TC-containing wastewater [10]. The adsorption process is effective, simple to operate and does not produce toxic substances during the removal of TCs [11]. In addition, the membrane filtration technology has the characteristics of low cost and simple operation. However, adsorption and membrane treatment methods could enrich antibiotics rather than degrade them, inducing a risk of secondary pollution [12]. Among them, advanced oxidation processes (AOPs) can oxidize TCs to small molecules or even achieve complete mineralization, which has a bright application prospect [13].

In recent years, advanced oxidation based on peroxymonosulfate (PMS) has attracted much attention in the field of refractory organics removal from water due to their high oxidation capacity, wide range of active species, applicable pH and high selectivity [14–16]. Catalysts play a key role in the process of PMS activation and active species generation. Biochar (BC) prepared by pyrolysis of waste biomass integrates the advantages of a well-developed pore structure and large specific surface area [17] but suffers from insufficient active sites and poor catalytic activity. Interestingly, transition metals exhibit high catalytic activity [18,19]. Thus, combining transition metals with BC carriers to form transition-metal-decorated BC composites can not only form multiple active sites and effectively improve the catalytic capacity of the composites but also reduce metal ion leaching and improve recyclability.

Currently, the metals used for the activation of PMS are mainly Fe, Cu, Mn, Co, etc. [20–22]. Among them, Cu-based composites exhibit the advantages of abundant source, low toxicity, high activity and stability [23]. As is well known, Cu/CuO-supported catalysts were widely employed for environmental applications such as nitrophenols decomposition [24], electrochemical energy conversion [25] and nitroaromatic compound reduction [26]. Inspired by the above research, the Cu/CuO-decorated BC is supposed to be an ideal catalyst. Yet, the current BC-based catalysts prepared by direct impregnation of biomass with metal salts and co-pyrolysis suffer from lower metal loading, poorer catalytic activity and relatively higher leaching rate [27]. To address these challenges, in this study, Cu/CuO-decorated BC was prepared by the impregnation of BC (containing abundant surface functional groups) with metal salts, followed by re-pyrolysis. Moreover, the physicochemical properties of the Cu/CuO-BC, such as microscopic morphology, elemental composition, lattice structure and functional groups, were analyzed. Tetracycline hydrochloride (TC), as a typical TC antibiotic, was selected as the target contaminant. Furthermore, the effects of common co-existing anions and organic matter on TC degradation were investigated by Cu/CuO-BC-activated PMS. Most importantly, the dominant active species were identified, and the pathway of active species generation was deduced. This study is instructive for the degradation of antibiotics in water by PMS activation with BC-based catalysts.

2. Results and Discussion

2.1. Characterization of the Prepared Cu/CuO-BC Catalysts

2.1.1. Micromorphology and Specific Surface Area

The surface morphology of the initial BC and Cu/CuO-BC composites were analyzed by SEM, as shown in Figure 1. The morphology of pure BC showed a porous structure with a relatively smooth outer surface. As seen in Figure 1b–d, the surface morphologies of Cu/CuO-BC500, Cu/CuO-BC600 and Cu/CuO-BC700 became rough, with fine particulate matter distributed on the surface and in the pore channels, which might be due to the conversion of metal ions into metal and oxides during the pyrolysis process. The mapping profile of Cu/CuO-BC700 is shown in Figure 1, which reveals the uniform distribution of Cu, C, O and N in the composite catalyst. The Cu element was more uniformly distributed on the surface of BC, which was beneficial to the catalytic activity.

The specific surface area of catalysts has an important effect on the activity, and in general, the larger the specific surface area, the higher the activity [28]. The specific surface area of BC was determined as 22.57 m²/g. Interestingly, the specific surface area of Cu/CuO-BC increased from 41.43 to 192.64 m²/g with the annealing temperature. Obviously, the pure BC had the smallest specific surface, and the specific surface area of Cu/CuO-BC700 was about 8.5 times larger than that of pure BC. More pyrolysis gas was generated at higher annealing temperatures, which facilitated the formation of pore structure [28]. As a result, the porous structure contributed to the increase of specific surface area. The pores of the catalyst after modification seemed more abundant from SEM images, which facilitated compound migration and removal.

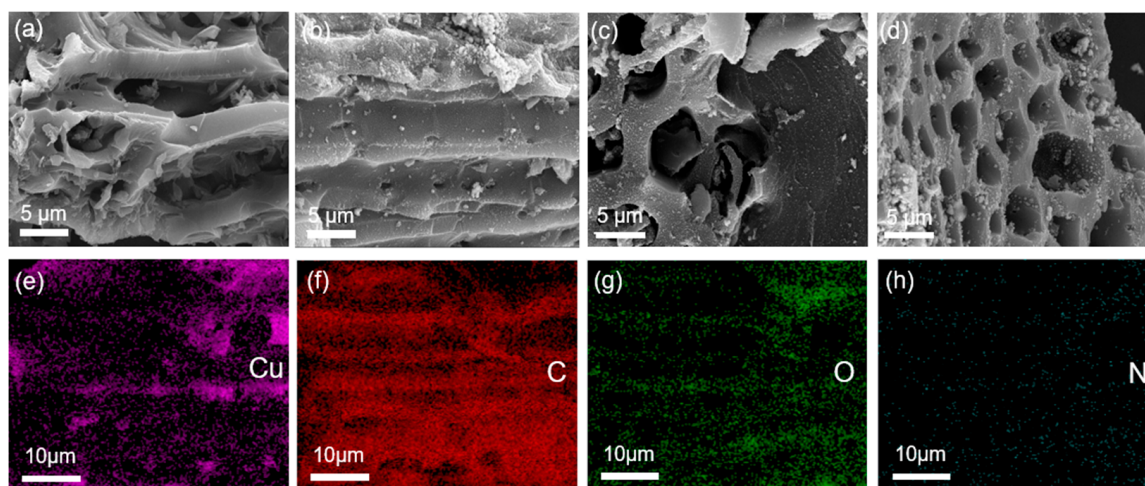


Figure 1. SEM images of (a) BC, (b) Cu/CuO-BC500, (c) Cu/CuO-BC600, (d) Cu/CuO-BC700; (e–h) Elements (Cu, C, O, N) mapping patterns of Cu/CuO-BC700.

2.1.2. Phase Structure and Composition

The structural analysis of BC and Cu/CuO-BC700 was performed by X-ray diffractometer, as shown in Figure 2. The Cu/CuO-BC700 exhibited obvious diffraction peaks of Cu at $2\theta = 43.39^\circ$, 50.43° and 74.13° , corresponding to the typical (111), (200) and (220) crystal planes (Cu PDF#04-0836) [29], respectively. Diffraction peaks of Cu were found at 35.41° and 38.70° , which were identified as typical (002) and (111) crystal planes of CuO (CuO PDF#48-1548) [30]. It can be inferred that the conversion of Cu^{2+} in the impregnated solution to CuO and Cu monomers occurred during the high-temperature pyrolysis.

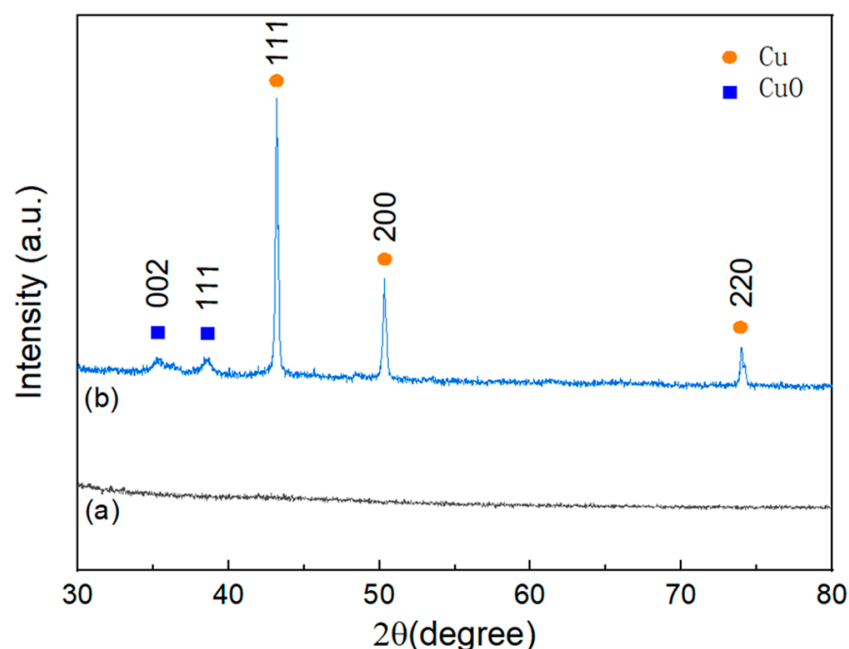


Figure 2. X-ray diffraction patterns of (a) BC and (b) Cu/CuO-BC700.

2.1.3. Surface Functional Groups

The FTIR spectra of the original BC and Cu/CuO-BC700 were examined, and the results are shown in Figure 3. For BC and Cu/CuO-BC700, the characteristic peaks at 1597 , 1355 , 1093 , 805 , 875 and 469 cm^{-1} in the mid-high and low-frequency band regions represented the C=C/C=O, C-H, C-O-C, C-H (1,2,4 substituted), aromatic C-H and Si-O-Si stretching vibration peaks on BC surface, respectively [31–33]. The original BC was rich

in surface functional groups, which contributed to the hydrophilicity and dispersibility of the catalyst. For Cu/CuO-BC700, the characteristic peak at 619 cm^{-1} in the low-frequency region was caused by the stretching vibration of the Cu-O bond [34], which proved the successful loading of Cu into the BC.

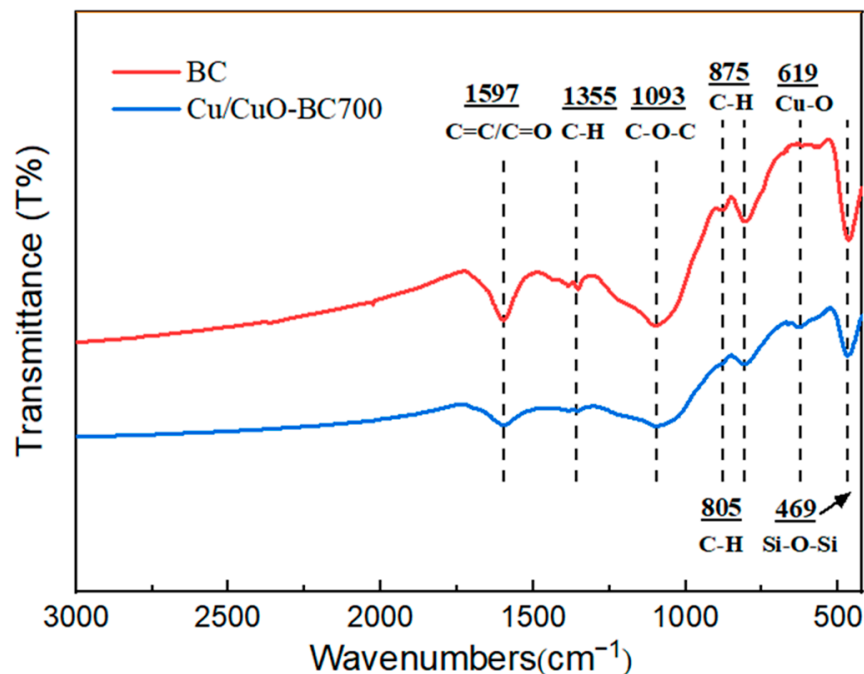


Figure 3. Infrared spectra of BC and Cu/CuO-BC700.

2.2. Catalytic Performance of Cu/CuO-BC

2.2.1. The Effect of Pyrolysis Temperature

The effect of pyrolysis temperature on the activity of the catalysts was investigated. As shown in Figure 4a, the adsorption efficiency of TC on Cu/CuO-BC increased from 18.9% to 29.4% as the preparation temperature rose from 500 to 700 °C, which was positively correlated with the specific surface area. At the oxidative degradation stage, the TC concentration rapidly decreased in the first 10 min and then slowly decreased from 10 to 30 min. The TC degradation efficiency was also increased with the rise of pyrolysis temperature (from 500 to 700 °C), increasing from 75.2% to 93.2% at 30 min. When only PMS (0.5 mM) was added, the removal rate of TC was 27.8% in 30 min, which relied on the active species produced by chemical bond breakage in PMS. To further investigate the degradation kinetics of TC by PMS activation with Cu/CuO-modified BC, the first-order kinetic model was employed, and the fitting results are shown in Figure 4b. Apparently, all degradation data followed the first-order kinetic model ($R^2 = 0.89\text{--}0.97$). The degradation rate constant of MB by PMS was only 0.0115 min^{-1} , while that of Cu/CuO-BC500/PMS, Cu/CuO-BC600/PMS and Cu/CuO-BC700/PMS systems were 0.0455, 0.0519 and 0.0921 min^{-1} , respectively. With the same TC/PMS concentration and lower catalyst dosage, the removal efficiency in the Cu/CuO-BC700/PMS system at 30 min was comparable with that of the Fe/Mn-bimetallic-composite-modified biochar/PMS system at 60 min. The degradation rate constant by the Cu/CuO-BC700/PMS system was about twice as high as that of the Fe/Mn-modified biochar/PMS system [35]. In summary, the Cu/CuO-BC700 (referred to as Cu/CuO-BC) exhibited the desired activity for PMS activation and TC degradation.

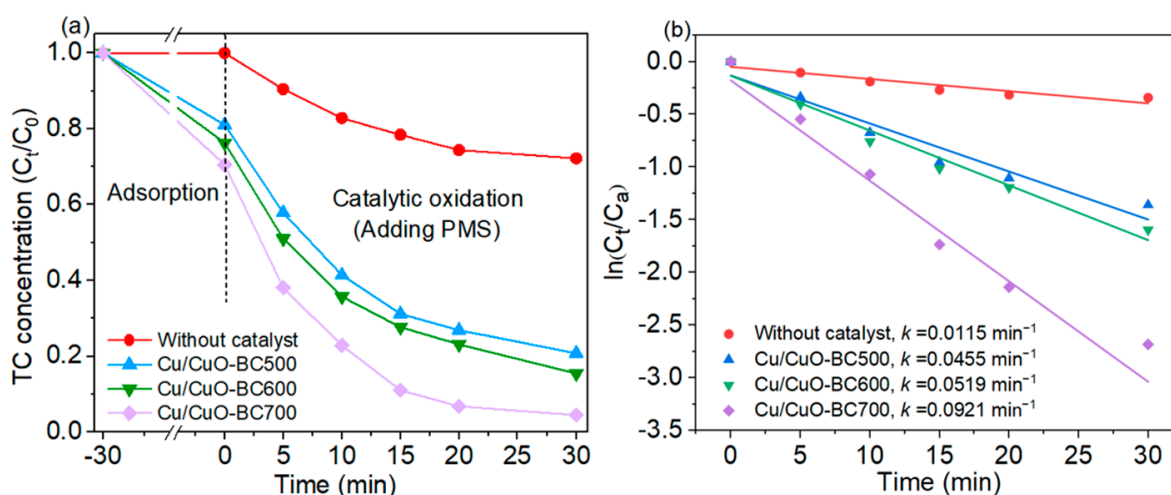


Figure 4. (a) TC adsorption and degradation process with Cu/CuO-modified BC; (b) Linear fit of degradation data by first-order kinetic model.

2.2.2. The Recyclability of Cu/CuO-BC

The reusability of the catalyst is closely related to practical applicability. The recyclability of Cu/CuO-BC was evaluated by a recycling experiment. As shown in Figure 5, the TC degradation efficiency was reduced from 93.2% to 83.5% after using it five times. The results indicated that the Cu/CuO-BC prepared in this study exhibited relatively good reusability. In addition, the leaching amount of metal ions in the solution was detected by ICP-MS. The results showed that the leaching amount of Cu^{2+} was 0.22 mg/L, much lower than the Chinese Sanitary Standard for Domestic Drinking Water GB 5749-2022 [36]. After five consecutive cycles, the catalysts were analyzed by XRD, and the results are shown in Figure S1. Compared with the fresh Cu/CuO-BC patterns, the diffraction peaks of the Cu and CuO loaded on BC decreased slightly after usage, which might be attributed to the leaching of copper ions. The positions of diffraction peaks of Cu/CuO-BC remained unchanged before and after PMS activation, indicating that the catalyst was stable during repeating utilization.

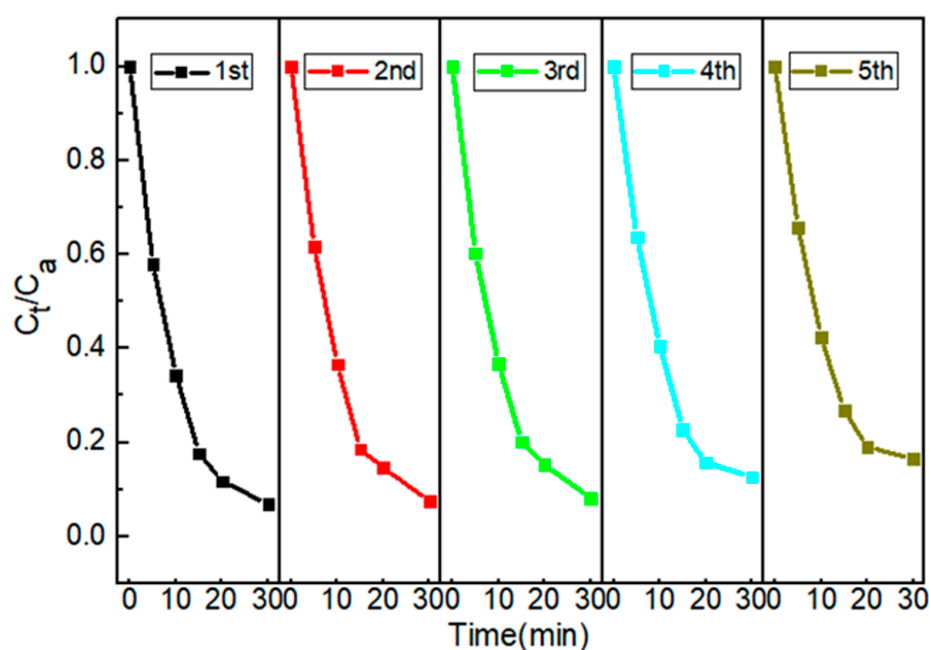


Figure 5. TC degradation with the cycle of Cu/CuO-BC.

2.2.3. The Effect of Co-existing Anions and Humic Acid

The common anions and natural organic matter (NOM) in water have potential influences on the oxidation process. The effects of three co-existing anions (Cl^- , HCO_3^- , H_2PO_4^-) and humic acid (HA, a common NOM) on TC adsorption and degradation were investigated, and the results were shown in Figure 6. Compared to the degradation stage, TC adsorption on Cu/CuO-BC was less affected by the co-existing anions and humic acid. The falling ranges of TC adsorption efficiency in the presence of Cl^- , HCO_3^- and H_2PO_4^- (0.5–2.0 mM) were 0.9–2.8%, 2.5–6.7% and 4.3–9.2%, respectively. The negatively charged anions might adsorption on Cu/CuO-BC, resulting in the reduction of TC adsorption efficiency. Interestingly, the HA enhanced the TC adsorption process. The adsorption efficiency increased from 33.8% to 39.9% in the range of HA concentration (0.5–2.0 mM). The numerous hydroxyl groups on the HA surface could interact with TC via complexation reactions. Thus, the TC removal by adsorption was enhanced with co-existing HA.

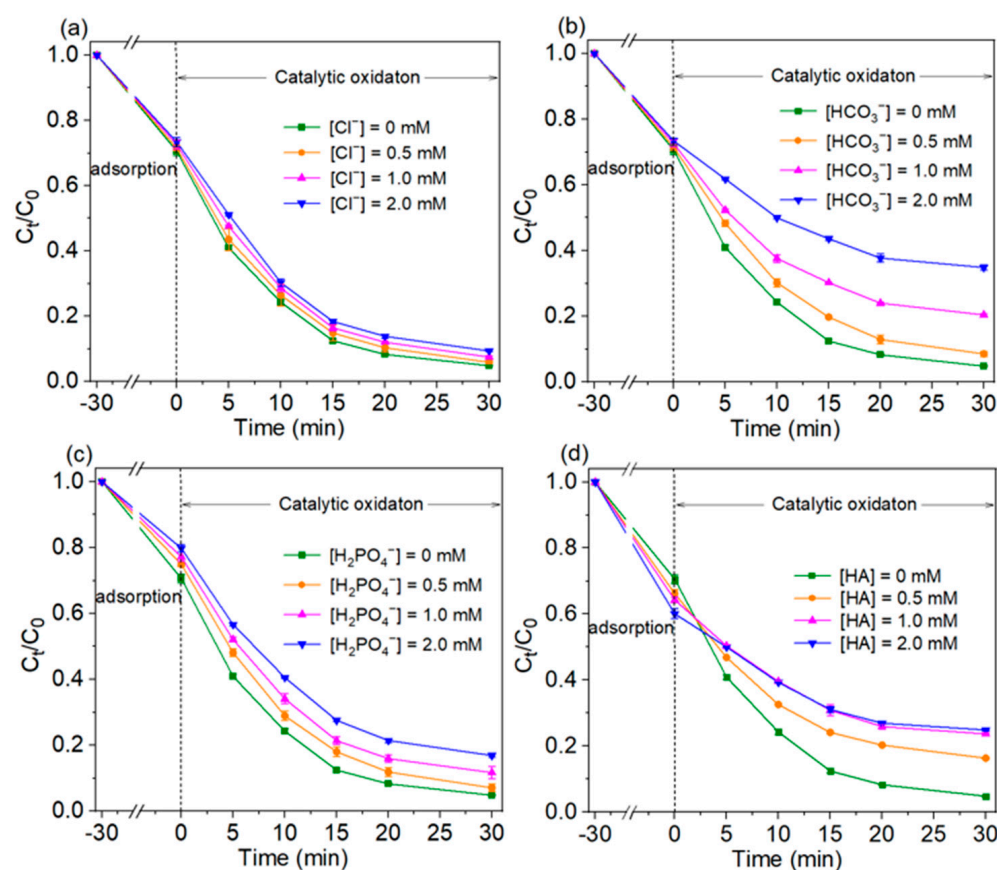
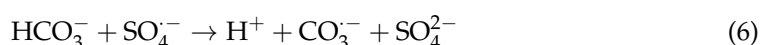


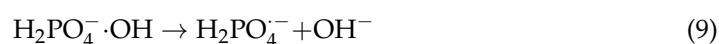
Figure 6. Effect of co-existing anions (a) Cl^- , (b) HCO_3^- , (c) H_2PO_4^- and (d) HA on TC removal.

The effect of Cl^- on TC degradation was small. As the Cl^- concentration was increased from 0 to 2.0 mM, the degradation efficiency of TC decreased from 93.2% to 86.7% at 30 min. The degradation efficiency decreased by only 6.2%. In this process, Cl^- would react with the active species to generate Cl-containing oxidants. The co-existing Cl^- in solution might converted to $\text{Cl}_2^{\bullet-}$, Cl^\bullet , and HClO (Equations (1)–(5)). The generated $\text{Cl}_2^{\bullet-}$ ($E^0 = 2.0$ V) and Cl^\bullet ($E^0 = 2.4$ V) possessed slightly weaker oxidation capacity than $\text{SO}_4^{\bullet-}$ ($E^0 = (2.5\text{--}3.1$ V)) [37] but were still capable of degrading TC. Thus, the system was less effective in degrading TC but still maintained a high removal rate. However, HCO_3^- in solution was able to inhibit the degradation of TC significantly. The degradation efficiency of TC decreased from 93.2% to about 50% when the concentration was increased from 0 to 2.0 mM. The HCO_3^- not only consumed the $\text{SO}_4^{\bullet-}$ in solution but also generated $\text{CO}_3^{\bullet-}$

with less oxidation ability ($E^0 = 1.78$ V) than the $\cdot\text{OH}$ (Equations (6) and (7)) [38]. The concentration of the strongly oxidative species in the system is reduced.



As shown in Figure 6c, the degradation of TC at 30 min decreased from 93.2% to 75.3% with increasing H_2PO_4^- concentration (0–2.0 mM). The H_2PO_4^- adsorbed on the metal sites of the catalyst to form complexes, thus reducing the catalytic active sites. Furthermore, H_2PO_4^- could trap the $\text{SO}_4^{\bullet-}$ and $\cdot\text{OH}$ [38] (Equations (8) and (9)), which in turn reduced the catalytic activity. In the present experiment, the degradation of TC was not significantly inhibited, probably because H_2PO_4^- reduced the activation energy of PMS, accelerated the production of active species, and slowed down the inhibitory effect of H_2PO_4^- on TC degradation. In addition, the degradation efficiencies of TC within 30 min were 93.2%, 77.2%, 65.2% and 59.5%, respectively, at HA concentrations of 0, 2.0, 4.0 and 8.0 mg/L. As the concentration of HA increased, the inhibition effect was enhanced. The reactive functional groups, such as amine, carboxyl and phenolic hydroxyl groups in HA, reacted with the active species [39]. As a result, the steady-state concentration of the active species was reduced, and the degradation efficiency of TC was inhibited.



2.3. Mechanism of TC Degradation by PMS Activation with Cu/CuO-BC

2.3.1. Contribution of Active Species for TC Degradation

In order to investigate the contribution of active species to the TC degradation by PMS activated with Cu/CuO-BC, typical chemical probes (trapping agents) were used to identify the active species during the reaction process. Ethanol (EtOH) was used as a trapping agent for $\text{SO}_4^{\bullet-}$ ($k_{\text{SO}_4^{\bullet-}} = (1.6\text{--}7.8) \times 10^7/\text{M}\cdot\text{s}$) and $\cdot\text{OH}$ ($k_{\text{OH}} = (1.2\text{--}2.8) \times 10^9/\text{M}\cdot\text{s}$), the tertiary butanol (TBA) was employed as a trapping agent for $\cdot\text{OH}$ ($k_{\text{OH}} = (3.8\text{--}7.6) \times 10^8/\text{M}\cdot\text{s}$), and furfuryl alcohol (FFA) was selected as trapping agents for $^1\text{O}_2$ ($k_{^1\text{O}_2} = 1.2 \times 10^8/\text{M}\cdot\text{s}$) and $\cdot\text{OH}$ ($k_{\text{OH}} = 1.5 \times 10^{10}/\text{M}\cdot\text{s}$) [39]. Additionally, benzoquinone (BQ) was used for trapping $\text{O}_2^{\bullet-}$ ($k_{\text{O}_2^{\bullet-}} = 9.8 \times 10^8/\text{M}\cdot\text{s}$) and $\cdot\text{OH}$ ($k_{\text{OH}} = 6.6 \times 10^9/\text{M}\cdot\text{s}$) [40]. The results are shown in Figure 7. After adding 500 mM EtOH and TBA to the reaction solution, the TC removal efficiency decreased from 93.2% to 28.2% and 45.4% within 30 min, respectively. It indicated the TC degradation was inhibited significantly, indicating the $\text{SO}_4^{\bullet-}$ and $\cdot\text{OH}$ played an important role in the TC degradation. Furthermore, the addition of FFA and BQ resulted in a decrease in TC removal efficiency—as low as 24.8% and 20.9%, respectively. Considering the trapped $\cdot\text{OH}$ by FFA and BQ, the $\text{O}_2^{\bullet-}$ and $^1\text{O}_2$ played a minor role in TC degradation.

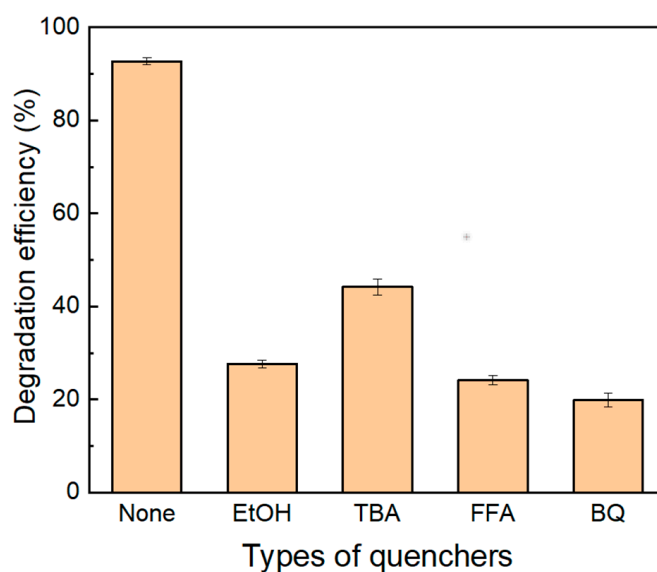


Figure 7. TC removal with different scavengers by Cu/CuO-BC in PMS system.

2.3.2. The Possible Generation Mechanism of Active Species

In order to investigate the possible generation mechanism of active species, X-ray photoelectron spectroscopy (XPS) analysis was carried out on the virginal and used Cu/CuO-BC. The full spectrum of Cu/CuO-BC is shown in Figure S2. The main elements of Cu/CuO-BC were Cu, O, N and C, which remained unchanged before and after PMS activation, indicating the composition stability of Cu/CuO-BC. High-resolution XPS spectra of the metal element Cu of the virginal and used Cu/CuO-BC are shown in Figure 8. The Cu 2p spectrum of virginal Cu/CuO-BC catalyst has a characteristic peak at 932.6 and 934.2 eV, which represents the characteristic peaks of Cu⁰ and Cu²⁺ [41]. The composing proportion of Cu⁰ (43.9%) was approximately twice that of Cu²⁺ (22.7%), revealing the main existing species of Cu⁰ in the catalyst, which was consistent with the XRD phase analysis. In the Cu 2p spectrum of the used Cu/CuO-BC, the characteristic peak at 932.6 eV was ascribed to Cu⁰, while the characteristic peaks at 933.3 eV and 934.2 eV were corresponded to Cu⁺ and Cu²⁺, respectively. Notably, the proportion of Cu²⁺ increased to 37.15% after the reaction, indicating the conversion of Cu²⁺ during the TC degradation process. In addition, the characteristic peak of Cu⁺ was detected, suggesting the occurrence of a reduction reaction from Cu²⁺. Meanwhile, Cu⁺ was also oxidized to Cu²⁺ by PMS, thus maintaining high catalyst activity via the valence cycle of Cu⁺ and Cu²⁺.

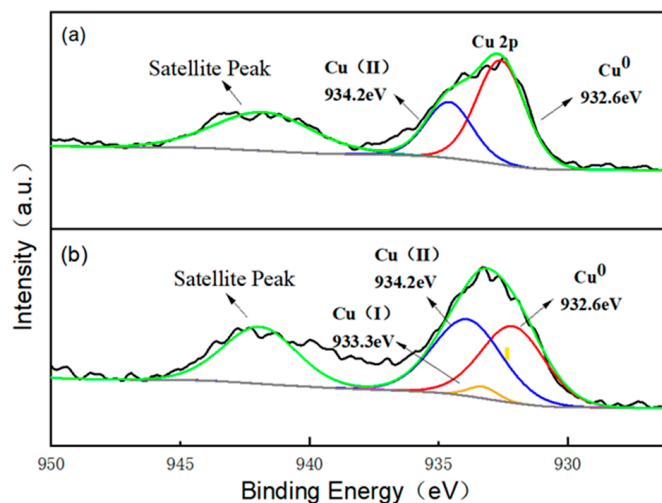


Figure 8. High-resolution XPS spectra of Cu 2p of Cu/CuO-BC (a) before and (b) after PMS activation.

Based on the above results, the generation mechanism of active species via PMS activation with Cu/CuO-BC was proposed, as shown in Figure 9. The Cu^0 site in Cu/CuO-BC coordinated with TC through the surface Cu-N bond, where the N site belonged to the amino group ($-\text{NH}_2$) in TC [42]. PMS could directly interact with the newly generated complexes with electron transfer from PMS to Cu^0 , thus facilitating PMS activation. Meanwhile, the Cu^0 converted to Cu^+ via redox reaction, producing $\cdot\text{OH}$ and $\text{SO}_4^{\bullet-}$ (Equations (10) and (11)). Also, Cu^+ could directly react with HSO_5^- to generate $\text{SO}_4^{\bullet-}$ and $\cdot\text{OH}$ (Equation (12)). Afterwards, the $\text{SO}_4^{\bullet-}$ could further combine with H_2O to generate $\cdot\text{OH}$ (Equation (11)). In addition, BC-based catalysts can produce $\text{O}_2^{\bullet-}$ and $^1\text{O}_2$ via Equations (13) and (14). Then, the formed H_2O_2 reacted with $\cdot\text{OH}$ to form $\text{HO}_2\cdot$ (Equation (15)), which in turn converted to $\text{O}_2^{\bullet-}$ (Equation (16)) [43]. Importantly, the Cu-N bridge formed between Cu^{2+} and TC, which accelerated PMS activation and electrons transferred to the Cu^{2+} sites, reducing Cu^{2+} to Cu^+ (Equation (17)). Consequently, the $\text{Cu}^+/\text{Cu}^{2+}$ cycle on the catalyst surface maintained the high utilization of PMS, contributing to the effective degradation of TC.

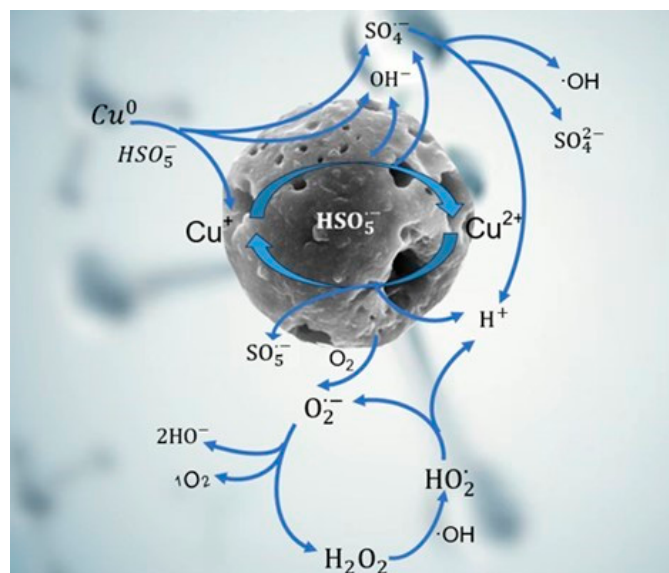
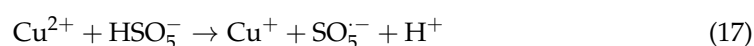
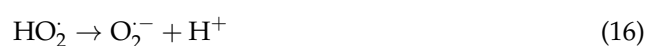
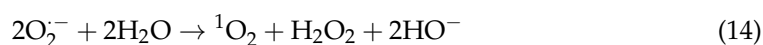
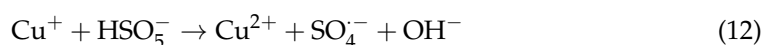


Figure 9. Mechanism of the process of activation of PMS by Cu/CuO-BC to produce active species.



3. Materials and Methods

3.1. Chemicals

The peanut shell used in this study is the peanut shell waste of agricultural products. The solutions were prepared with ultrapure water. Copper sulfate ($\text{CuSO}_4 \cdot 5\text{H}_2\text{O}$) and TC with analytical grade were purchased from Shanghai Zehuasheng Technology Co., LTD (Shanghai, China) and Tianjin Biaotai Technology Development Co., LTD (Tianjin, China), respectively. Ethanol and PMS were supplied by Tianjin Jinke Fine Chemical Research Institute. Tert-butyl alcohol (TBA) and sodium dihydrogen phosphate (NaH_2PO_4) were also analytically pure, which were obtained from Tianjin Damao chemical reagent factory. Sodium bicarbonate (NaHCO_3) and sodium chloride (NaCl) were purchased from Tianjin Biaotai and Guangfu Technology Development Co., LTD (Tianjin, China). Furfuryl alcohol and benzoquinone were purchased from Aladdin Reagent (Shanghai) Co., LTD (Shanghai, China).

3.2. Preparation of Cu/CuO-BC Catalysts

In the first stage, peanut shell was used to prepare biochar-based catalyst. The peanut shells were weighed and washed with deionized water 3 times and placed in an oven at $60\text{ }^\circ\text{C}$ to dry to a constant weight. Then, peanut shells were crushed by a ball mill to obtain a finer peanut shell powder, which was sieved through 100 mesh and then placed in a tube furnace for pyrolysis with a heating rate of $10\text{ }^\circ\text{C}/\text{min}$, pyrolysis temperature of $300\text{ }^\circ\text{C}$ and pyrolysis time of 2 h. The black powder was removed after the tube furnace cooled down naturally to room temperature. In the second stage, modified BC was prepared by impregnation pyrolysis. After the beaker was filled with 1.0 g of peanut-shell-derived powder, 200 mL of CuSO_4 solution with 0.1575 M was added to make the mass ratio (2) of Cu to the powder. The mixture was stirred continuously with a magnetic stirrer for 24 h. The supernatant was removed after standing, and the impregnated powder was dried and placed in a tube furnace for pyrolysis at 500, 600 and $700\text{ }^\circ\text{C}$ with a heating rate of $10\text{ }^\circ\text{C}/\text{min}$ and a pyrolysis time of 2 h. The preparation was completed when the tube furnace cooled down naturally to room temperature. For better comparison with the modified biochar, the powder obtained from the first stage also experienced re-pyrolysis at $500\text{ }^\circ\text{C}$ without impregnation, which was named BC. The acquired modified biochar-based catalysts were marked as Cu/CuO-BC500, Cu/CuO-BC600 and Cu/CuO-BC700, respectively.

3.3. Characterization

The prepared BC and Cu/CuO-BC were analyzed by scanning electron microscopy (TESCAN MIRA LMS, Brno, Czech Republic) for microscopic morphology. The samples were scanned under energy scattering spectrometer (EDS) to detect the elemental composition on BC and Cu/CuO-BC surface. The specific surface area and pore size distribution of the BC-based catalysts were determined using a specific surface analyzer (McMurray-Tick Gemini VII 2390, McMurray, PA, USA). The surface functional groups of catalysts were analyzed using Fourier infrared spectroscopy (Thermo Fisher Nicolet iS10, Waltham, MA, USA). X-ray diffraction (Rigaku Smartlab SE, Akishima, Japan) was used to determine the structure and crystalline phase of the catalysts with a conventional angle of $10\text{--}80^\circ$ and a scanning speed of $10\text{ }^\circ/\text{min}$. X-ray photoelectron spectroscopy (Thermo Scientific ESCALAB 250Xi, Waltham, MA, USA) was used to detect the elemental composition of the catalysts and their valence structure. Electron paramagnetic resonance (EPR) spectroscopy measurement was conducted by a spectrometer (Bruker E500, Mannheim, Germany) at room temperature in the PMS system mediated by Cu/CuO-BC.

3.4. TC Degradation Experiment

In a 250 mL conical flask, 10 mL of 200 mg/L TC solution was added, diluted to 100 mL with deionized water, shaken well and then 0.01 g of catalyst powder was added. The catalyst was ultrasonically dispersed using an ultrasonic cleaner and then sampled at 300 r/min at a reaction temperature of $25\text{ }^\circ\text{C}$ after stirring for 30 min to reach adsorption equilibrium.

PMS solution (2.0 mL) with a concentration of 25 mM was added after adsorption equilibrium, and samples were taken at 5, 10, 15, 20 and 30 min, respectively. The samples were filtered through a 0.22 μm polyethersulfone membrane, and the reaction was terminated by adding the same volume of 0.1 M sodium thiosulfate and then loaded into liquid phase vials for measurement. The TC concentration was detected by ultra-performance liquid chromatography (HPLC, SIL-30AC) with a C18 column (15 cm \times 4.6 mm) following mobile phases: A: 0.1% formic acid aqueous solution; B: acetonitrile (chromatographic purity), VA:VB = 85:15, with gradient elution; flow rate: 0.1 mL/min; column temperature: 30 $^{\circ}\text{C}$; injection volume: 10. The effects of co-existing anions on TC degradation were studied in the presence of single NaCl, NaHCO_3 and NaH_2PO_4 . The effect of NOM on TC removal was investigated with humic acid. The TC relative concentration was expressed as C_t/C_a or C_t/C_0 , where the C_t , C_a and C_0 were the concentrations of adding PMS for t min, reaching adsorption equilibrium and initial concentration, respectively. The pseudo-first-order kinetic model was described as $\ln(C_t/C_a) = -K \times t$, where K is the rate constant and t is the degradation time.

4. Conclusions

In this study, Cu/CuO-BC catalysts were optimally prepared and characterized by a modified impregnation pyrolysis method with peanut shells as raw material. The research focused on the performance and mechanism of Cu/CuO-BC for TC degradation by PMS activation. The successful loading of Cu/CuO and the increased specific surface area (192.64 m^2/g) facilitated the TC removal, achieving the degradation efficiency of 93.2% at 30 min with the kinetic constant of 0.0921 min^{-1} . The inhibition of TC degradation by co-existing anions (0.5–2.0 mM) followed the order of $\text{HCO}_3^- > \text{H}_2\text{PO}_4^- > \text{Cl}^-$. Also, HA had an inhibitory effect on TC degradation. The free radical ($\cdot\text{OH}$ and $\text{SO}_4^{\bullet-}$) pathway played a dominant role in TC degradation. The $\cdot\text{O}_2^-$ and $^1\text{O}_2$ were also involved in TC removal. The cycling of $\text{Cu}^+/\text{Cu}^{2+}$ on the catalyst surface kept the high activity and good recyclability. The TC degradation efficiency was reduced from 93.2% to 83.5% after using five times. The prepared Cu/CuO-BC in this study was a highly active and environmentally friendly catalyst, which was of great value for new compound degradation in water.

Supplementary Materials: The following supporting information can be downloaded at <https://www.mdpi.com/article/10.3390/catal13091246/s1>. Figure S1: XRD patterns of Cu/CuO-BC before and after recycling experiment; Figure S2: XPS Survey scan of Cu/CuO-BC (a) before and (b) after PMS activation.

Author Contributions: Conceptualization, J.Z. and N.L.; methodology, Y.W.; software, H.L.; validation, Y.W., H.L. and J.Z.; formal analysis, J.Z. and Y.W.; investigation, Y.W.; resources, Y.W.; data curation, H.L.; writing—original draft preparation, J.Z.; writing—review and editing, N.L.; visualization, H.L.; supervision, J.Y.; project administration, J.Y.; funding acquisition, S.W. All authors have read and agreed to the published version of the manuscript.

Funding: This work was supported by the Research Project of the Tianjin Education Commission (2019KJ111).

Data Availability Statement: Data are available within the article.

Conflicts of Interest: There are no conflict of interest to declare.

References

1. Serra, A.; Gómez, E.; Michler, J.; Philippe, L. Facile cost-effective fabrication of Cu@Cu₂O@CuO-microalgae photocatalyst with enhanced visible light degradation of tetracycline. *Chem. Eng. J.* **2021**, *413*, 127477. [[CrossRef](#)]
2. Huang, X.; Chen, C.; Zeng, Q.; Ding, D.; Gu, J.; Mo, J. Field study on loss of tetracycline antibiotics from manure-applied soil and their risk assessment in regional water environment of Guangzhou, China. *Sci. Total Environ.* **2022**, *827*, 154273. [[CrossRef](#)] [[PubMed](#)]
3. Kaiser, R.A.; Polk, J.S.; Datta, T.; Parekh, R.R.; Agga, G.E. Occurrence of antibiotic resistant bacteria in urban karst groundwater systems. *Water* **2022**, *14*, 960. [[CrossRef](#)]

4. Wang, Y.; Zhao, X.; Zang, J.; Li, Y.; Dong, X.; Jiang, F.; Wang, N.; Jiang, L.; Jiang, Q.; Fu, C. Estimates of dietary exposure to antibiotics among a community population in East China. *Antibiotics* **2022**, *11*, 407. [[CrossRef](#)]
5. Chen, X.; Yang, Y.; Ke, Y.; Chen, C.; Xie, S. A comprehensive review on biodegradation of tetracyclines: Current research progress and prospect. *Sci. Total Environ.* **2022**, *814*, 152852. [[CrossRef](#)]
6. Żyła, R.; Ledakowicz, S.; Boruta, T.; Olak-Kucharczyk, M.; Foszpańczyk, M.; Mrozińska, Z.; Balcerzak, J. Removal of tetracycline oxidation products in the nanofiltration process. *Water* **2021**, *13*, 555. [[CrossRef](#)]
7. Lama, G.; Meijide, J.; Sanromán, A.; Pazos, M. Heterogeneous advanced oxidation processes: Current approaches for wastewater treatment. *Catalysts* **2022**, *12*, 344. [[CrossRef](#)]
8. Mansouri, F.; Chouchene, K.; Roche, N.; Ksibi, M. Removal of pharmaceuticals from water by adsorption and advanced oxidation processes: State of the art and trends. *Appl. Sci.* **2021**, *11*, 6659. [[CrossRef](#)]
9. Amangelsin, Y.; Semenova, Y.; Dadar, M.; Aljofan, M.; Bjørklund, G. The impact of tetracycline pollution on the aquatic environment and removal strategies. *Antibiotics* **2023**, *12*, 440. [[CrossRef](#)]
10. Zhang, S.; Zheng, K.; Xu, G.; Liang, B.; Yin, Q. Enhanced removal of tetracycline via advanced oxidation of sodium persulfate and biochar adsorption. *Environ. Sci. Pollut. R* **2022**, *29*, 72556–72567. [[CrossRef](#)]
11. Hao, D.; Chen, Y.; Zhang, Y.; You, N. Nanocomposites of zero-valent iron@biochar derived from agricultural wastes for adsorptive removal of tetracyclines. *Chemosphere* **2021**, *284*, 131342. [[CrossRef](#)] [[PubMed](#)]
12. Polak, D.; Zielińska, I.; Szwast, M.; Kogut, I.; Małolepszy, A. Modification of ceramic membranes with carbon compounds for pharmaceutical substances removal from water in a filtration-Adsorption system. *Membranes* **2021**, *11*, 481. [[CrossRef](#)]
13. Wang, X.; Jing, J.; Zhou, M.; Dewil, R. Recent advances in H₂O₂-based advanced oxidation processes for removal of antibiotics from wastewater. *Chin. Chem. Lett.* **2023**, *34*, 107621. [[CrossRef](#)]
14. Wang, X.; Zhang, C.; Li, D.; Sun, Y.; Ren, J.; Sun, J.; Yang, D. Theoretical study of local S coordination environment on Fe single atoms for peroxydisulfate-based advanced oxidation processes. *J. Hazard. Mater.* **2023**, *454*, 131469. [[CrossRef](#)]
15. Manos, D.; Miserli, K.; Konstantinou, I. Perovskite and spinel catalysts for sulfate radical-based advanced oxidation of organic pollutants in water and wastewater systems. *Catalysts* **2020**, *10*, 1299. [[CrossRef](#)]
16. Li, Z.; Sun, Y.; Liu, D.; Yi, M.; Chang, F.; Li, H.; Du, Y. A Review of Sulfate Radical-Based and Singlet Oxygen-Based Advanced Oxidation Technologies: Recent Advances and Prospects. *Catalysts* **2022**, *12*, 1092. [[CrossRef](#)]
17. Li, Y.; Shang, H.; Cao, Y.; Yang, C.; Feng, Y.; Yu, Y. High performance removal of sulfamethoxazole using large specific area of biochar derived from corncob xylose residue. *Biochar* **2022**, *4*, 11. [[CrossRef](#)]
18. Ghanbari, F.; Jaafarzadeh, N. Graphite-supported CuO catalyst for heterogeneous peroxydisulfate activation to oxidize Direct Orange 26: The effect of influential parameters. *Res. Chem. Intermed.* **2017**, *43*, 4623–4637. [[CrossRef](#)]
19. Wang, Y.; Cao, D.; Liu, M.; Zhao, X. Insights into heterogeneous catalytic activation of peroxydisulfate by Pd/g-C₃N₄: The role of superoxide radical and singlet oxygen. *Catal. Commun.* **2017**, *102*, 85–88. [[CrossRef](#)]
20. Feng, M.; Xu, Z.; Bai, X.; Lin, K.; Zhang, M. Exploration the mechanisms underlying peroxydisulfate activation by nano-cubic spinel M₂MnO₄ nanoparticles for degrading trichloroethylene. *Chem. Eng. J.* **2022**, *446*, 137394. [[CrossRef](#)]
21. Manos, D.; Papadopoulou, F.; Margellou, A.; Petrakis, D.; Konstantinou, I. Heterogeneous activation of persulfate by LaMO₃ (M= Co, Fe, Cu, Mn, Ni) perovskite catalysts for the degradation of organic compounds. *Catalysts* **2022**, *12*, 187. [[CrossRef](#)]
22. Yang, Z.; Hou, J.; Wu, J.; Miao, L. Mesoporous carbon framework supported Fe-Cu-Mn oxides as an efficient peroxydisulfate catalyst for the control of harmful algal blooms: Synergism of Fe-Cu-Mn and role of mesoporous carbon. *Chem. Eng. J.* **2023**, *461*, 141877. [[CrossRef](#)]
23. Ding, Y.; Li, D.; Zuo, S.; Guan, Z.; Ding, S. Boron-doping accelerated Cu(II)/Cu(I) cycle for enhancing peroxydisulfate activation. *Sep. Purif. Technol.* **2022**, *282*, 120086. [[CrossRef](#)]
24. Mashentseva, A.A.; Barsbay, M.; Zdorovets, M.V.; Zhelto, D.A.; Güven, O. Cu/CuO composite track-Etched membranes for catalytic decomposition of nitrophenols and removal of As (III). *Nanomaterials* **2020**, *10*, 1552. [[CrossRef](#)]
25. Zhang, D.; Li, Y.; Liu, L.; Duan, L.; Ren, Z.; Xu, S.; Chen, L.; Guo, H.; Huang, Y.; Shi, L.; et al. Cu/CuO_x@C composite as a high-efficiency electrocatalyst for oxygen reduction reactions. *Catalysts* **2022**, *12*, 1515. [[CrossRef](#)]
26. Jin, Z.; Liu, C.; Qi, K.; Cui, X. Photo-reduced Cu/CuO nanoclusters on TiO₂ nanotube arrays as highly efficient and reusable catalyst. *Sci. Rep.* **2017**, *7*, 39695. [[CrossRef](#)]
27. Li, M.; Li, P.; Zhou, Q.; Lee, S.L.J. A mini review on persulfate activation by sustainable biochar for the removal of antibiotics. *Materials* **2022**, *15*, 5832. [[CrossRef](#)] [[PubMed](#)]
28. Kim, C.; Zhu, C.; Aoki, Y.; Habazaki, H. Heteroatom-doped porous carbon with tunable pore structure and high specific surface area for high performance supercapacitors. *Electrochim. Acta* **2019**, *314*, 173–187. [[CrossRef](#)]
29. Peng, L.; Wang, Y.; Masood, I.; Zhou, B.; Wang, Y.; Lin, J.; Qiao, J.; Zhang, F. Self-growing Cu/Sn bimetallic electrocatalysts on nitrogen-doped porous carbon cloth with 3D-hierarchical honeycomb structure for highly active carbon dioxide reduction. *Appl. Catal. B-Environ.* **2020**, *264*, 118447. [[CrossRef](#)]
30. Liang, Y.C.; Li, T.H. Sputtering-assisted synthesis of copper oxide–titanium oxide nanorods and their photoactive performances. *Nanomaterials* **2022**, *12*, 2634. [[CrossRef](#)] [[PubMed](#)]
31. Ouyang, D.; Chen, Y.; Yan, J.; Qian, L.; Han, L.; Chen, M. Activation mechanism of peroxydisulfate by biochar for catalytic degradation of 1, 4-dioxane: Important role of biochar defect structures. *Chem. Eng. J.* **2019**, *370*, 614–624. [[CrossRef](#)]

32. Ahmed, M.B.; Zhou, J.L.; Ngo, H.H.; Guo, W. Insight into biochar properties and its cost analysis. *Biomass Bioenerg.* **2016**, *84*, 76–86. [[CrossRef](#)]
33. Liang, G.; Wang, Z.; Yang, X.; Qin, T.; Xie, X.; Zhao, J.; Li, S. Efficient removal of oxytetracycline from aqueous solution using magnetic montmorillonite-biochar composite prepared by one step pyrolysis. *Sci. Total Environ.* **2019**, *695*, 133800. [[CrossRef](#)] [[PubMed](#)]
34. Zhong, Q.; Lin, Q.; Huang, R.; Fu, H.; Zhang, X.; Luo, H.; Xiao, R. Oxidative degradation of tetracycline using persulfate activated by N and Cu codoped biochar. *Chem. Eng. J.* **2020**, *380*, 122608. [[CrossRef](#)]
35. Liang, F.; Liu, Z.; Jiang, X.; Li, J.; Xiao, K.; Xu, W.; Chen, X.; Liang, J.; Lin, Z.; Li, M.; et al. NaOH-modified biochar supported Fe/Mn bimetallic composites as efficient peroxymonosulfate activator for enhance tetracycline removal. *Chem. Eng. J.* **2023**, *454*, 139949. [[CrossRef](#)]
36. Wang, G.; Shen, J.; Wei, S.; Cai, D.; Liu, J. Identification of Heavy Metals and Organic Micropollutants in Drinking Water Sources in Typical Villages and Towns in Northeast China. *Molecules* **2022**, *27*, 8033. [[CrossRef](#)] [[PubMed](#)]
37. Qin, W.; Fang, G.; Wang, Y.; Zhou, D. Mechanistic understanding of polychlorinated biphenyls degradation by peroxymonosulfate activated with CuFe₂O₄ nanoparticles: Key role of superoxide radicals. *Chem. Eng. J.* **2018**, *348*, 526–534. [[CrossRef](#)]
38. Zhao, Z.; Zhao, J.; Yang, C. Efficient removal of ciprofloxacin by peroxymonosulfate/Mn₃O₄-MnO₂ catalytic oxidation system. *Chem. Eng. J.* **2017**, *327*, 481–489. [[CrossRef](#)]
39. Yang, Y.; Banerjee, G.; Brudvig, G.W.; Kim, J.H.; Pignatello, J.J. Oxidation of organic compounds in water by unactivated peroxymonosulfate. *Environ. Sci. Technol.* **2018**, *52*, 5911–5919. [[CrossRef](#)]
40. Das, B.; Devi, M.; Deb, S.; Dhar, S.S. Boosting photocatalytic property of graphitic carbon nitride with metal complex fabrication for efficient degradation of organic pollutants. *Chemosphere* **2023**, *323*, 138230. [[CrossRef](#)]
41. Nie, W.; Mao, Q.; Ding, Y.; Hu, Y.; Tang, H. Highly efficient catalysis of chalcopyrite with surface bonded ferrous species for activation of peroxymonosulfate toward degradation of bisphenol A: A mechanism study. *J. Hazard. Mater.* **2019**, *364*, 59–68. [[CrossRef](#)] [[PubMed](#)]
42. Mi, X.; Zhong, H.; Zhang, H.; Xu, S.; Li, Y.; Wang, H.; Crittenden, J.C. Facilitating redox cycles of copper species by pollutants in peroxymonosulfate activation. *Environ. Sci. Technol.* **2022**, *56*, 2637–2646. [[CrossRef](#)] [[PubMed](#)]
43. Zhao, J.; Wang, Y.; Li, N.; Wang, S.; Yu, J.; Li, X. Efficient degradation of ciprofloxacin by magnetic γ -Fe₂O₃-MnO₂ with oxygen vacancy in visible-light/peroxymonosulfate system. *Chemosphere* **2021**, *276*, 130257. [[CrossRef](#)]

Disclaimer/Publisher's Note: The statements, opinions and data contained in all publications are solely those of the individual author(s) and contributor(s) and not of MDPI and/or the editor(s). MDPI and/or the editor(s) disclaim responsibility for any injury to people or property resulting from any ideas, methods, instructions or products referred to in the content.